ACS OMEGA

Open Access

http://pubs.acs.org/journal/acsodf

Article

Blighia sapida Waste Biochar in Batch and Fixed-Bed Adsorption of Chloroquine Phosphate: Efficacy Validation Using Artificial Neural Networks

Adejumoke Abosede Inyinbor,* Deborah Temitope Bankole,* and Abimbola Peter Oluyori

Cite This: *ACS Omega* 2024, 9, 12564−12574

Read Online

ACCESS | Metrics & More | Article Recommendations | Supporting Information

ABSTRACT: The present study investigated the potency of biochar prepared from *Blighia sapida* seedpods (BSSPs) in the uptake of chloroquine phosphate (CQP) from single-component batch and multicomponent fixed-bed adsorption systems. BSSPs presented a highly porous structure with a BET surface area of 1122.05 m^2/g, to which adsorption efficiency correlated. The Dubinin−Radushkevich isotherm energy was obtained as 129.09 kJ/mol, confirming the chemisorption nature of the BSSP-CQP adsorption system. The efficiency of the artificial neural network (ANN) was evaluated using the lowest mean square error (MSE = 7.27) and highest correlation coefficient (R^2 = 0.9910). A good agreement between the experimental results and the ANN-predicted data indicated the efficiency of the model. The percentage removal of 95.78% obtained for the column adsorption studies indicated the effectiveness of BSSPs in a multicomponent system. The mechanism of the interaction proceeded via hydrogen bonding and electrostatic attraction. This was confirmed by the high desorption efficiency (69.11%) with a HCl eluent. The degree of reversibility was found to be 2.95, indicating the reusability potential of BSSPs. BSSPs are therefore considered multilayered adsorbents with potential applications in pharmaceutical wastewater treatment.

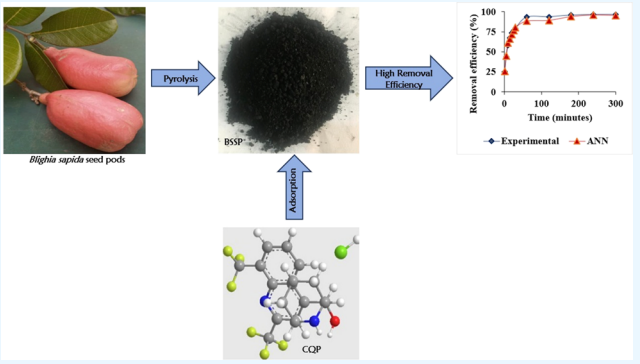

1. INTRODUCTION

Pharmaceuticals are complex molecules developed to preserve animal and human health.[1,2] These molecules, on the other hand, are part of emerging contaminants discovered in the environment that have the potential to harm both humans and the environment. The extent of their toxicity has become a major concern as effects upon human and aquatic organism exposure are yet to be fully understood.[3] Chloroquine phosphate (CQP) is a member of the quinoline group, which has bactericidal, antipyretic, and antiseptic properties.[4] CQP has been primarily used in the treatment of malaria, and its enhanced antitumor activity has led to its use in cancer therapy. In addition, CQP has been used as an antifungal and for the treatment of rheumatic diseases and management of influenza A/H5N1, HIV, and SARS-CoV viruses.[5−7]

Regardless of the numerous benefits, CQP has been associated with serious side effects such as hypokalemia, blindness, cardiac arrest, arrhythmias, retinopathy, cerebral edema, renal failure, and, in the case of overdose, death of the embryo in treatments during pregnancy.[4,8,9] Extensive use and overproduction of pharmaceuticals such as CQP can lead to their release into aquatic systems via sewage effluents, pharmaceutical industrial wastewater, and hospital effluents.[10,11] Given their lipophilic nature and resistance to degradation, pharmaceuticals are persistent and hence a serious concern.[11] In a bid to achieve a cleaner environment and sustainable community goals, a less expensive, adaptable, and effective wastewater treatment technique is required. Adsorption of various water pollutants using agricultural wastes has captivated the interest of environmental scientists.[12−15] This is because agrowastes are readily available, amenable, effective, and low-cost materials suitable as adsorbent precursors.

The adsorption process is a complex process that is influenced by several operational parameters. Modeling such complex processes with simple linear multivariate correlations is difficult.[16] The artificial neural network (ANN) is a model that can incorporate mathematical functions into nonlinear and linear systems. The ANN is superior to conventional models in terms of simplicity, capacity, and speed.[16−18] Although the forecast and prediction usually made using the conventional

Received: July 27, 2023
Revised: November 29, 2023
Accepted: December 13, 2023
Published: March 6, 2024

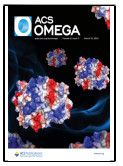

adsorption data treatment techniques can be considered effective, a validation using artificial intelligence such as the ANN is superior. In addition, the use of the ANN to predict the adsorption efficiency of pharmaceuticals onto adsorbents from agrowastes is scarce, and therefore, it is one of the values of this study.

This novel study therefore surveys the following line of thoughts: baseline batch adsorption of CQP from aqueous media using acid-activated biochar prepared from *Blighia sapida* seedpods (BSSPs) was carried out. The equilibrium and kinetic adsorption data were fitted by using the isothermal and kinetic models. The adsorption data were further fitted and validated using the ANN, and desorption studies were used to assess the strength of the BSSP-CQP bonds. Furthermore, we investigated the antagonist and synergistic effects of a multicomponent system via fixed-bed adsorption for the feasibility of industrial applications. This was achieved by testing the efficacy of BSSPs on CQP removal in the presence of other contaminants via column adsorption. The effects of the column flow rate, BSSP bed height, and CQP initial concentration were all investigated to establish the conditions for effective removal. This study established the possibility of BSSP efficiency in real pharmaceutical industrial wastewater applications.

2. MATERIALS AND METHODS

2.1. Collection, Pretreatment, and Acid Activation of *B. sapida* Wastes. *B. sapida* wastes were locally sourced from the Omu Aran community, in Kwara State, Nigeria (Latitude 8°8′24.82″ N, Longitude 5°5′46.73″E). Deionized water was utilized to thoroughly clean the obtained wastes, and they were then dried in an oven for 24 h at 105 °C. An Armfield hammermill FT2-A (serial number: 35404001) was used to reduce the particle size. 98% orthophosphoric acid was added to the sample in a ratio of 1:3. The mixture was heated until a paste was formed and charred at 350 °C for 90 min in a muffle furnace. The resulting biochar was washed with deionized water until a neutral pH was attained and dried in the oven at 105 °C for 24 h. A BSSP label was attached to the prepared biochar, which was then stored for later use.

2.2. Pharmaceutical Compounds and Reagents. The pharmaceutical company May & Baker located in Lagos, Nigeria, graciously gifted the chloroquine phosphate (batch no. 19098C3RT), ibuprofen (batch no. 1201/19SA-2993), ciprofloxacin (batch no. 105-200705-1), and lumefantrine (batch no. 21021LU3R11) used in this research. Additionally, only analytical-grade reagents and chemicals were used, while all solutions in this experiment were prepared with deionized water.

2.3. Characterization of BSSPs. The pH point of zero charge (pH_{pzc}) was determined by adjusting 50 mL of 0.1 M NaCl between pH 2 and 10 with HCl and NaOH for acidic and basic medium, respectively. 0.1 g of BSSPs was introduced to each of the preadjusted NaCl solutions. The mixture was stirred for 24 h, and the final pH was recorded. The pH_{pzc} value was determined as the intersection of the curve from the plot of ($pH_{final} - pH_{initial}$) vs $pH_{initial}$.[19,20] Other parameters such as percentage moisture content, volatile matter, ash content, and total fixed carbon were analyzed using the methods described by Ekpete et al. and Bello et al.[7,21] The functional groups present on the surface of BSSPs were investigated using a Fourier transform infrared (FTIR) model (Nicolet iS10) in the range of 4000−400 cm^{-1}. The BET surface area analysis was carried out using a micrometric porosity and surface area analyzer. The surface morphology and topography of BSSPs before and after CQP uptake were obtained by using scanning electron microscopy (SEM) (model: JEOL JSM-7600F, Japan) with an accelerating voltage ranging 10.0 kV, and an image at 500× magnification was selected for discussion.[22]

2.4. Adsorption Studies. *2.4.1. Batch Adsorption Conditions for CQP Uptake onto BSSPs.* Different adsorption experimental conditions were investigated for batch studies. Parameters such as pH (2, 4, 6, 8, and 10), initial CQP concentration (10, 20, 30, 40, and 50 mg/L), temperature (25, 35, 45, and 55 °C), and BSSP dosage (0.05, 0.10, 0.15, 0.20, and 0.25 g) were investigated. The adsorption processes were carried out in 250 mL conical flasks with 100 mL of CQP solution and 0.10 g of BSSP adsorbent, and a temperature-controlled water bath shaker was used for the entire time necessary to attain equilibrium. The supernatant was separated from the mixture, and the concentration of CQP after adsorption was estimated using a UV−visible spectrophotometer. A 0.1 M solution of hydrochloric acid and 0.1 M sodium hydroxide were employed to modify the pH of 100 mL of CQP solution for acidic and basic media, respectively. The optimal pH was then used throughout the experiment. Equation 1 was used to calculate the amount of CQP adsorbed onto BSSPs at different time intervals, and eq 2 was used to evaluate the removal efficiency, where C_o and C_e are the initial and equilibrium concentrations of CQP, respectively, V is the volume of the adsorbate, q_t is the quantity adsorbed at time t, and W is the mass of the BSSP adsorbent.[15,23,24]

$$q_t = \frac{(C_o - C_t)V}{W} \tag{1}$$

$$\%Re = \left\{\frac{C_o - C_e}{C_o}\right\} \times 100 \tag{2}$$

2.4.2. Development of Optimal Conditions for Artificial Neural Network Prediction. The artificial neural networks (ANNs) are models made up of layers (input and output) that are linked by nodes. ANN topography is composed of layers, the number of neurons that act as processing units in each layer, and the transfer functions.[16,17,24] This segment aimed to develop an ANN model that could successfully predict the efficiency of CQP adsorption with the best fit. In this work, the ANN model was developed in (MATLAB 2016a) mathematical software using a three-layered back-propagation neural network. The model was developed using the obtained datasets from the experimental procedure. The input variables include pH, initial CQP concentration, contact time, temperature, and BSSP dosage, while the adsorption efficiency (%) obtained from the input variables was used as the target. A total of 1,308 datasets were obtained from the effects of operational variables such as pH (2−10), initial CQP concentration (10−50 mg/L), contact time (5 min−equilibrium time), temperature (25−55 °C), and BSSP dosage (0.05−0.25 g) and their corresponding adsorption efficiencies. These datasets were divided into 70% (916 datasets), 15% (196 datasets), and 15% (196 datasets) for training, validation, and testing, respectively. The Levenberg−Marquardt algorithm was used to evaluate the best fit by varying the number of neurons in the hidden layer between 1 and 20. The hidden neuron with the lowest mean square error (7.27) and highest correlation coefficient (0.9910)

https://doi.org/10.1021/acsomega.3c05008
ACS Omega 2024, 9, 12564−12574

was selected in varying the activation functions (*Purelin*, *Tansig*, and *Logsig*). Also, the activation function with the highest correlation coefficient (0.9855) was then used to predict the adsorption efficiency. In summary, the network with the optimal parameters (5-11-1) was then used to predict the adsorption efficiency.

2.4.3. Composition of the Simulated CQP Multicomponent Effluent. Batch adsorption studies of a single-component system involve the removal of one pollutant. However, industrial wastewater contains various pollutant molecules that can interact and compete with each other. In the case of pharmaceutical wastewater, these molecules are components of drug actives and other drug excipients used in the manufacturing process. However, there can be antagonistic, synergistic, and noninteraction between these molecules, which can make an adsorption process complicated.[25,26] This segment was investigated to assess the efficiency of BSSPs for the uptake of CQP in the presence of other drug excipients. Two simulated multicomponent pharmaceutical effluents contain several drug excipients that are commonly found in untreated pharmaceutical effluents. The simulation was carried out following the idea of Lima et al. 2019 and Saucier et al. 2015.[27,28] The component ratio was also developed according to the Handbook of Pharmaceutical Excipients.[29] The simulated CQP multicomponent effluent's composition is presented in Table 1.

Table 1. Components of Simulated Pharmaceutical Effluents

	concentration (mg/L)	
wastewater contents	effluent A	effluent B
phosphate	20	40
lumefantrine	5	10
ibuprofen	5	10
ciprofloxacin	5	10
sucrose	10	20
starch	5	10
sodium sulfate	5	10
aluminum oxide	5	10
calcium carbonate	10	20

2.4.4. Fixed-Bed Adsorption Conditions and Operation Parameters for CQP Uptake onto BSSPs. We conducted the fixed-bed adsorption experiments on a pilot scale using a 35 cm length × 2.5 cm inner diameter column.[1,30,31] The BSSP sample was packed between two layers of glass wool (2 cm each) at the top and bottom of the column to ensure an even flow of the influent and to prevent the adsorbent from flowing out. The CQP solution of known concentration was fed into the column, while the outlet solution was sampled by taking 10 cm^3 at different time intervals. Fixed-bed parameters such as BSSP bed height (1 and 2 cm), column flow rate (6 and 12 mL/min), and initial CQP concentration (25 and 50 mg/L) were analyzed. Breakthrough curves, which express CQP concentration with respect to time, can explain the packed bed's performance. The breakthrough time t_b, time (t_s), and exhaustion time (t_e) were calculated at C_e = 0.5 and 0.9. The values were extracted from the graph of the plot of $\frac{C_t}{C_o}$ versus C_o. Equations 3a and 3b were used to calculate the maximum adsorption capacity of BSSPs (q_s and q_b in mg/g), where Q denotes the column's flow rate, w is the adsorbent mass, C_o is the initial CQP concentration, and C_t is the CQP concentration at time t. The obtained data from experiments were modeled using the Yoon−Nelson and Thomas models, to obtain additional information on the column's performance.[32,33]

$$q_s = \frac{C_o Q t_s}{w} \tag{3a}$$

$$q_b = \frac{C_o Q t_b}{w} \tag{3b}$$

2.5. Desorption Studies of the BSSP-CQP System. After the adsorption of CQP onto BSSPs, the spent adsorbent was immediately rinsed with deionized water to eliminate the unadsorbed CQP layer on the BSSP's surface. The spent BSSP was contacted with four eluents: 0.1 M hydrochloric acid (HCl), deionized water, 0.1 M sodium hydroxide (NaOH), and 0.1 M sodium chloride (NaCl). The desorption experiments were conditioned at 26 °C, 1 h, 130 rpm, 0.1 g of BSSP, and 40 mL for each of the eluents. The desorption efficiency was calculated using eq 4. The degree of reversibility was also investigated by calculating the desorption index (DI) using eq 5, where q_{de} and q_{ad} are the quantity desorbed by each of the eluents and quantity adsorbed during the adsorption processes, respectively[34]

$$\text{desorption efficiency (\%)} = \frac{q_{de}}{q_{ad}} \times 100 \tag{4}$$

$$\text{desorption index} = \frac{\text{\% CQP adsorbed}}{\text{\% CQP left on BSSP after desorption}} \tag{5}$$

3. RESULTS AND DISCUSSION

3.1. Adsorbent Characterization. The pH point of zero charge (pH_{pzc}) is the point at which the material's surface charge is zero. At pH values above pH_{pzc}, the adsorbent's surface is negatively charged, favoring the adsorption of positively charged molecules and vice versa.[20,35] As indicated in Figure S1, pH_{pzc} was determined to be 3.00. The moisture, ash, and volatile matter content values obtained were all significantly low, indicating that BSSPs are a suitable adsorbent for use in wastewater treatment.[36] BSSPs demonstrated a highly porous structure with a BET surface area of 1122.05 m^2/g, which was connected to the adsorption efficiency. Furthermore, the topography of the BSSP revealed unique interior pores, which are critical for efficient adsorption.

3.2. Batch Adsorption and Effects of Operational Parameters. *3.2.1. Effects of pH.* The pH of a solution significantly impacts interactive sorption.[14,37] Pharmaceuticals exist in the anionic form at pH above pK_a and the neutral form at pH below pK_a. CQP has three pK_a values of 4.0, 8.10, and 10.20.[38] A maximum removal efficiency of 94.10% was obtained at pH 8, which was subsequently utilized for varying other parameters. High efficiencies of 76.08 and 96.10% were between pH 2 and 9. This could be explained as follows: the ionization constants of CQP are 8.10 and 10.20 corresponding to the nitrogen quinoline ring and diethylamino side chain nitrogen ring, respectively, while between pH 4 and 5, CQP is biprotonated.[39] BSSP is, however, cationic at pH below pH_{pzc} (3.0)[20,22,40] and can form hydrogen bonding with the basic sites of CQP. BSSPs can also exist as anionic at pH above 3.0.[41] The synergistic effect of various existences of CQP as

https://doi.org/10.1021/acsomega.3c05008
ACS Omega 2024, 9, 12564−12574

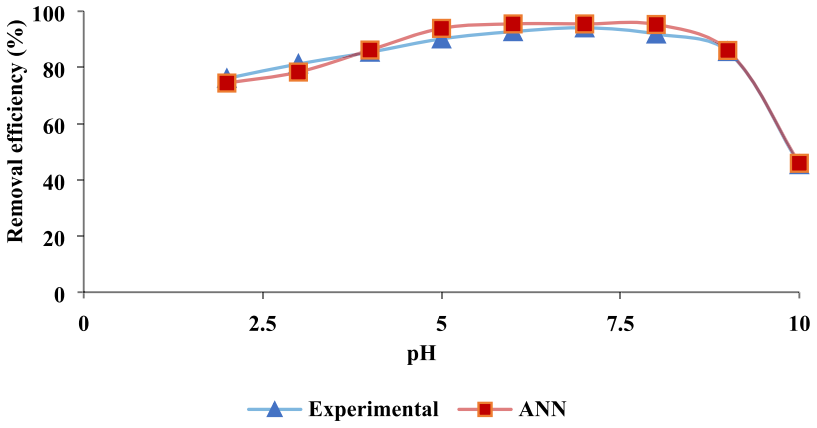

Figure 1. Effect of pH on the uptake of CQP onto BSSPs.

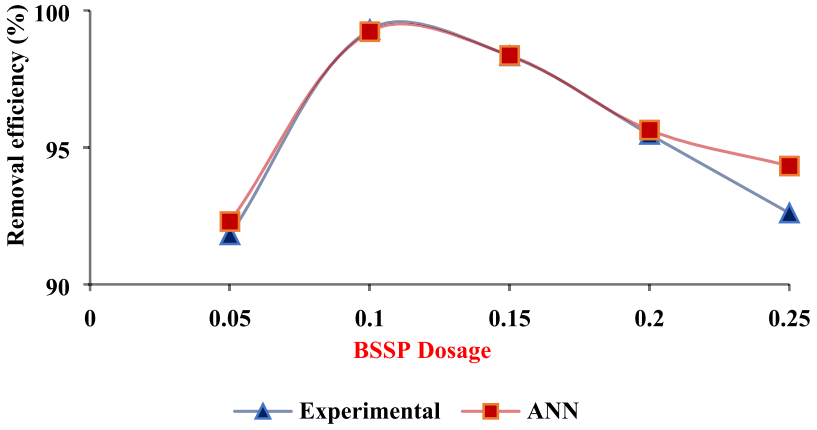

Figure 2. Effect of the BSSP dosage on the uptake of CQP removal.

Table 2. Kinetic Model Parameters of CQP Uptake onto BSSPs[a]

			initial CQP concentration (mg/L)				
			10	20	30	40	50
		$q_{e,exp.}$	9.48	17.08	26.71	35.58	45.46
kinetics	linear equation	evaluated parameters					
pseudo-first-order	$\log(q_e - q_t) = \ln q_e - K_1 t$	$q_{e,cal.}$	4.37	12.91	15.18	26.51	31.51
		K_1 (min)	0.02	004	0.02	0.02	0.02
		ARE	19.52	5.38	12.66	5.71	7.38
		χ^2	5.98	1.35	8.77	3.10	6.18
		R^2	0.9750	0.9931	0.9794	0.9930	0.9915
		$q_{e,cal.}$	9.64	17.79	27.85	37.73	48.31
		K_2 (min)	0.010	0.010	0.003	0.002	0.001
pseudo-second-order	$\frac{t}{q_t} = \frac{1}{K_2 q_e^2} + \frac{t}{q_e}$	ARE	0.2895	0.6903	0.7094	1.0084	1.0445
		χ^2	0.0028	0.0281	0.0464	0.1228	0.1681
		R^2	0.9991	0.9988	0.9992	0.9980	0.9979
		α_{EI} (mg/(g min))	20.67	36.65	41.88	53.99	61.51
Elovich	$q_t = \frac{1}{\beta}\ln(\alpha\beta) + \frac{1}{\beta}\ln t$	β_{EI} (g/mg)	0.8344	0.3361	0.2301	0.1549	0.1238
		R^2	0.9571	0.9429	0.9502	0.9443	0.9388
intraparticle diffusion	$q_t = K_{Diff} t^{0.5} + C$	C_1	1.6256	1.4822	1.3315	2.4518	3.1061
		K_{Diff} (mg/(g min$^{1/2}$))	1.2338	1.9805	3.1439	3.6592	4.7519
		R^2	0.9800	0.8581	0.9459	0.8855	0.8936
liquid film diffusion	$\ln\left(1 - \left(\frac{q_t}{q_e}\right)\right) = -K_{LFD} t + C$	K_{LFD}	0.02	0.03	0.02	0.03	0.03
		R^2	0.9783	0.9818	0.9788	0.9810	0.9638

[a] q_e is the quantity of CQP adsorbed at equilibrium (mg/g), q_t is the quantity of CQP adsorbed at time, t (mg/g), K_1 is the rate constant of pseudo-first-order (maccount), t is the time (min), K_2 is the rate constant of pseudo-second-order (g/(mg min)), α is the constant related to the rate of chemisorption, β is the constant that depicts the extent of the surface coverage, K_{Diff} is the rate constant for intraparticle diffusion (mg/(g min$^{1/2}$)), C extends insights into the boundary layer thickness, and K_{LFD} is the coefficient rate for the process corresponding to the BSSP particle size.

https://doi.org/10.1021/acsomega.3c05008
ACS Omega 2024, 9, 12564−12574

Table 3. Isotherm Model Parameters of CQP Uptake onto BSSPs[a]

model	linear equation	evaluated parameters	
Langmuir	$\frac{C_e}{q_e} = \frac{C_e}{q_{max}} + \frac{1}{q_{max}K_l}$	q_{max} (mg/g)	99.01
		K_L (L/mg)	0.3447
		R^2	0.9358
Freundlich	$\log q_e = \frac{1}{n}\log C_e + \log K_f$	K_F (mg/g)	24.74
		n	1.4112
		R^2	0.9729
Hasley	$\ln q_e = \frac{1}{n_H}\ln K_H - \frac{1}{n_H}\ln C_e$	$1/n_H$	0.7089
		K_H	0.0100
		R^2	0.9729
Hills	$\log \frac{q_e}{q_H - q_e} = n_H \log C_e - \log K_D$	n_H	1.0173
		K_D	1.5900
		q_H	99.01
		R^2	0.9550
Dubinin−Radushkevich	$\ln q_e = \ln q_m - A_{DRK}\varepsilon^2$	q_{DR} (mg/g)	51.99
	$\varepsilon = RT \ln\left[1 + \frac{1}{C_e}\right]$	E (kJ/mol)	129.09
	$E = -\left[\frac{1}{\sqrt{2A_{D-R}}}\right]$	R^2	0.9988

[a] C_o symbolizes the initial CQP concentration in mg/L, Ce represents the CQP concentration in mg/L, q_e represents the amount of CQP adsorbed per mass of BSSP in mg/g, q_m denotes the maximum monolayer adsorption capacity of BSSPs in mg/g, K_L denotes the Langmuir constant in L/mg, K_F denotes the Freundlich constant in mg/g, whose heterogeneity extent increases as the value approaches zero, n_H and K_D are Hill's isotherm constants, K_H is Hasley's isotherm constant, B is the Redlich-Peterson constant, q_{DR} is the theoretical adsorption isotherm saturation capacity in mg/g, and E denotes the mean free adsorption energy, which predicts the type of adsorption in kJ/mol.

well as multiple surface charges of BSSPs can explain the high efficiencies obtained between pH 2 and 9. Above pH 9, CQP is negatively charged, while the BSSP surface is negatively charged (pH above pH_{pzc}), resulting in electrostatic repulsion. Hence, a sharp drop in the removal efficiency from 94.10 to 45.40% was observed.[42] The comparison of experimental and ANN-predicted data for the influence of pH on CQP removal by BSSPs is shown in Figure 1. The comparison shows that the ANN model displayed an outstanding performance in predicting the data. Furthermore, the optimal ANN that gave the best prediction captured the system's experimental variability, as the predicted data trend is similar to the experimental data trend. This indicates that the network has the potential to predict real data.[43]

3.2.2. Effects of the BSSP Dosage. The percentage removal increased marginally from 91.81 to 99.30% as the BSSP dosage increased to 0.10 from 0.05 g/100 mL (Figure 2). This may be attributed to the rise in the number of active sites that are currently available as the BSSP dosage increased, which in turn increased the surface area, resulting in a higher percentage removal.[44] Also, the percentage removal decreased slightly as the dosage was further increased from 0.10 to 0.25 g (99.30−92.61%). This could be due to active site overlapping caused by excess BSSP particles.[45] The ANN prediction and experimental results as a function of the BSSP dosage showed that they were in good agreement.

3.2.3. Effects of the CQP Initial Concentration and Contact Time. Figure S2 presents the effect of contact time on the percentage removal of CQP at various concentrations (20, 30, 40, and 50 mg/L). For all of the investigated concentrations, CQP removal increased as the contact time increased. There was a rapid initial increase in the quantity adsorbed in the first 60 min, which slowed down until equilibrium was achieved. The rapid adsorption rate was ascribed to the fact that there are many existing adsorption sites on the BSSPs for CQP uptake at the beginning of adsorption. Adsorption rates slowed as adsorption sites became saturated.[13,46] The evaluation of the experimental results with ANN predictions, as shown in Figure S1, was found to be in good agreement.

3.3. Kinetic Studies of CQP Uptake onto BSSPs. Five kinetic models were used to predict the mechanism and possible rate-controlling steps of the BSSP-CQP adsorption system. The models of pseudo-first-order (PFO), pseudo-second-order (PSO), Elovich, intraparticle diffusion (ID), and liquid film diffusion (LFD) were studied. The linear plots of these models and values derived for their parameters are depicted in Table 2. The estimated correlation coefficients (R^2), Chi-square (χ^2), and average relative error (ARE) established that the PSO model better described the experimental data. The estimated errors for the PSO model were very low (0.002−0.17 for χ^2 and 0.29−1.04 for ARE). The R^2 values (0.9980−0.9991) were obtained to be close to unity across all the investigated concentrations, indicating the suitability of the PSO model.[32,47] The desorption coefficient (β_{EI}) for the Elovich model was discovered to decrease as the starting CQP concentration increased, whereas the chemisorption rate (α_{EI}) increased. Also, the values of α_{EI} are greater than those of β_{EI}, indicating that chemisorption governs the adsorption process.[48] The intercept (C) values, which predicted the thickness of the boundary layer for the ID model, increased from 1.6256 to 3.1061 across the investigated concentrations (10−50 mg/g). This suggested the contribution of the boundary layer to the mechanism of adsorption.[31] However, the R^2 values of liquid film diffusion are greater than those of the ID model, which indicated that external diffusion and surface diffusion dominated the adsorption process.[49,50] Similar findings from kinetic studies have been reported.[32,51]

3.4. Isothermal Studies on CQP Uptake onto BSSPs. Adsorption isotherms help describe the interactions of adsorbents and adsorbates at equilibrium. Each model reveals specific information, depending on individual underlying theories. The Hills, Langmuir, Hasley, Freundlich, and Dubinin−Radushkevich isotherms were selected to evaluate

https://doi.org/10.1021/acsomega.3c05008
ACS Omega 2024, 9, 12564−12574

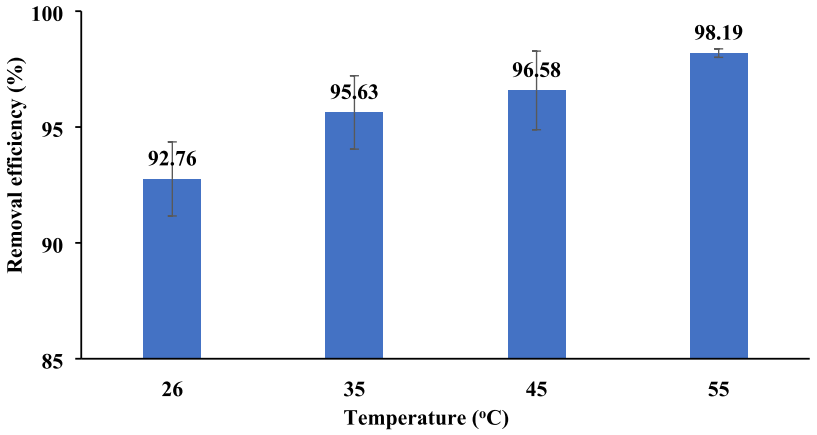

Figure 3. Effect of the temperature on the uptake of CQP onto BSSPs.

the BSSP-CQP adsorption system. The maximum monolayer adsorption capacity of the Langmuir isotherm was found to be 99.01 mg/g. The value of n for the Freundlich model was obtained to be greater than 1, which validated the favorability of the adsorption process.[52] The correlation coefficient (R^2 = 0.9729) of the Freundlich model was found to be larger than that of Langmuir (0.9358). This implied that multilayer adsorption occurred in the BSSP-CQP system. Also, the R^2 values of the Hasley isotherm were obtained to be 0.9729, while that of the Hill isotherm was obtained to be 0.9546 (lower than that of Hasley). This confirmed the multilayered nature of the BSSP-CQP adsorption system.[12] The Dubinin−Radushkevich isotherm adsorption energy (E) for the BSSP-CQP system was obtained to be 129.09 kJ/mol (higher than 8 kJ/mol), which indicated that the adsorption process is primarily through chemisorption.[53] The result agrees with some reported studies using activated carbon prepared from agricultural wastes.[54,55] Various evaluated isotherm parameters are listed in Table 3.

3.5. Temperature Effects and Thermodynamic Studies. The role of temperature in controlling the strength of the adsorptive force of interaction between adsorbents and adsorbates is very crucial.[47] The temperature effect on the removal of CQP onto BSSPs was investigated at 26, 35, 45, and 55 °C as shown in Figure 3. As the temperature increased, BSSP percentage removal also increased (92.76−98.19%); therefore, high temperature favored the adsorption system. This is because as the temperature of the adsorption system elevated, the mobility of the ions in solution increased, leading to increased interactions between BSSPs and CQP molecules.[56]

The ANOVA test and the posthoc test using the Duncan multiple range test (DMRT) were analyzed. The obtained P-value (0.072) was found to be greater than 0.05 (Table S6), which implied that there exists a significant difference among the investigated temperatures. Also, the DMRT analysis (Tables S7 and S8) showed that there is a slight difference between the percentages adsorbed at 26 and 35 °C, a slight difference between 35 and 45 °C, and a significant difference between 26 and 55 °C.

The entropy, Gibb's free energy, and enthalpy are thermodynamic concepts evaluated alongside adsorption isotherms, which provide further insight into the nature of the adsorbate−adsorbent interaction. Table S1 displays the calculated thermodynamic parameters. The negative values of $\Delta G°$ (−6.34 to −10.89 kJ/mol) established the adsorption process's spontaneity and feasibility. As the temperature increases, the process becomes more feasible. The positive value of $\Delta H°$ (+38.44 kJ/mol) established the BSP1-CQP system's endothermic nature, whereas the positive value of $\Delta S°$ (+149.83 J/K/mol) reflected the adsorption system's increased randomness.[57]

3.6. Postadsorption Analysis. Surface and morphological characterizations of BSSPs before and after CQP adsorption provided evidence of a successful adsorption process. The scanning electron microscopy revealed pores of different shapes and sizes before adsorption (Figure 4a). However, after the uptake of CQP (Figure 4b), these openings were observed to have been covered with what appeared like interwoven web-like matter. This is a result of the impregnation of the pores and attachment of CQP molecules, which is morphological evidence of the adsorption process.[58]

With the aid of Fourier transform infrared spectroscopy, the surface chemistry of BSSPs was examined both before and after the adsorption process. Figure 5 displays the FTIR spectra of BSSPs before and after CQP uptake. The main characteristics of the FTIR spectrum include the band at 3410 cm^{-1} associated with −OH and N−H stretching, a low intensity band at 2880 cm^{-1} associated with C−H stretching, sharp peaks at 1620 cm^{-1} associated with C═O, bands at 1460 cm^{-1} associated with the aliphatic C−H stretching, a weak peak at 1240 cm^{-1} associated with the C−O stretching of aryl esters and phenols or O−H deformation of COOH, and the band at 1090 cm^{-1} assigned to the C−O stretch.[59,60] The shifts in intensities observed confirmed the contribution of these functional groups in the adsorption system.[61]

3.7. Effects of Operational Parameters on Column Adsorption of CQP. *3.7.1. Effects of the Flow Rate.* While operational factors such as pH, bed height, and CQP initial concentration were kept steady at 8, 1 cm (equals 0.308 g of BSSP), and 50 mg/L, respectively, the flow rate was varied between 6 and 12 mL/min. At flow rates of 6 and 12 mL/min, as shown in Figure 7, when the flow rate was increased from 6 to 12 mL/min, the breakthrough time dropped from 790 to 240 min as illustrated in Figure S3. The amount of CQP adsorbed decreased as well, from 59142.86 to 14882.35 mg/g. This is because an elevation in the rate of flow decreased the time of physical contact between CQP and BSSPs. This causes the bulk of the CQP molecules to exit the column without proper contact with BSSP pores. As a result, the resistance mass transfer increases, creating an increased driving force in

https://doi.org/10.1021/acsomega.3c05008
ACS Omega 2024, 9, 12564−12574

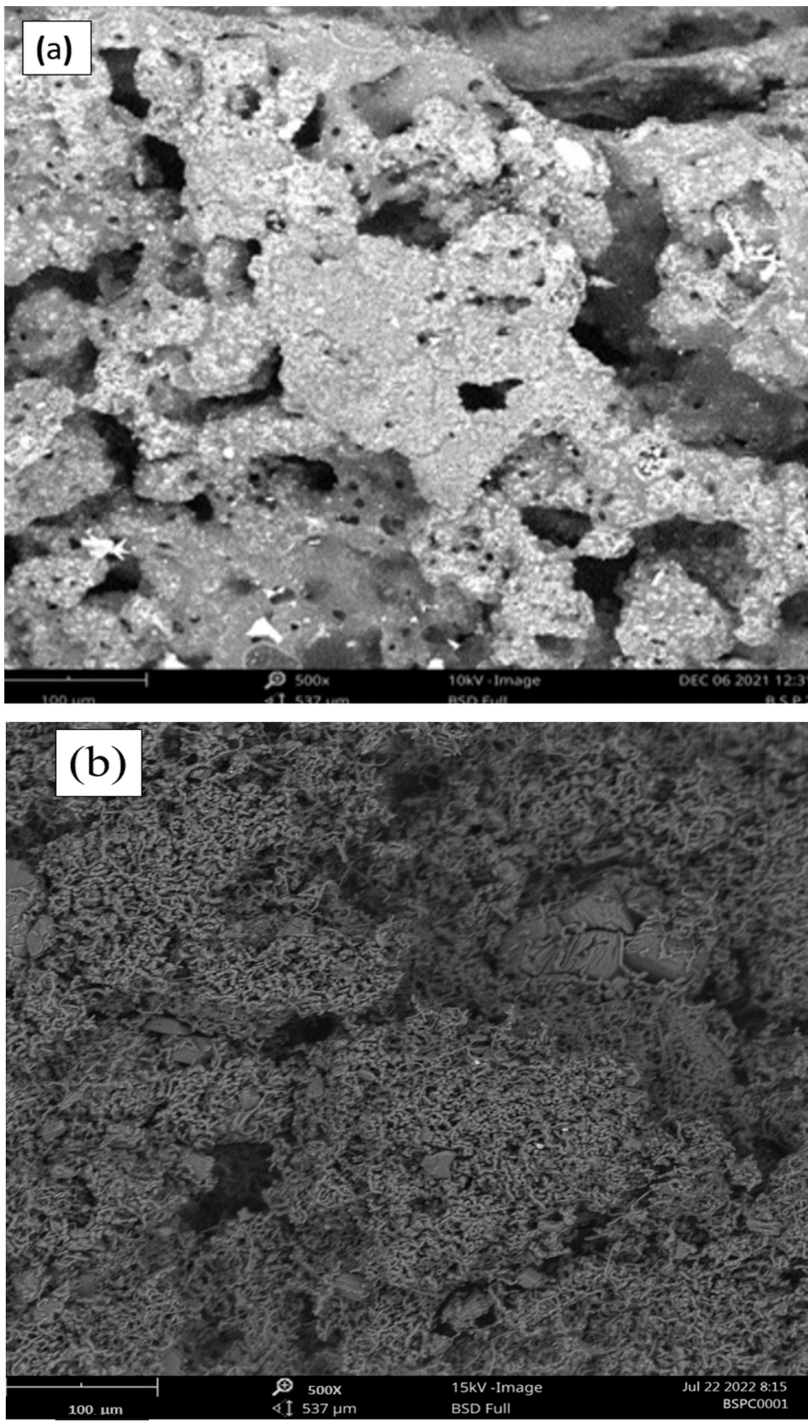

Figure 4. Surface morphology of the BSSP (a) before and (b) after the uptake of CQP.

the column and hence resulting in lower service time of the bed and decreased quantity adsorbed.[62]

3.7.2. Effects of the Initial Concentration. Figure S4 illustrates breakthrough curves for the effect of initial CQP concentration for 25 and 50 mg/L. pH, bed depth (0.308 g equiv of BSSP), and flow rate were all held at 8, 1, and 12 mL/min, respectively. The breakthrough and exhaustion times decreased from 15 to 12 min and 275 to 240 min, respectively, as the starting concentration increased from 25 to 50 mg/L. This could be because the higher initial CQP concentration raised the mass transfer driving force across the liquid film, resulting in earlier column exhaustion due to an accelerated adsorption rate.[63] Furthermore, an increase in the initial CQP concentration causes BSSP pores to get saturated more quickly, thus reducing the column exhaustion time.[64]

3.7.3. Effects of the Bed Height. The breakthrough curve for the uptake of CQP onto BSSPs at bed heights of 1 cm (0.308 g equiv of BSSP) and 2 cm (0.612 g equiv of BSSP) is shown in Figure S5. At 8, 50 mg/L, 6 mL/min, and 8 mg/L, the operational parameters pH and initial CQP concentration were maintained. T_b and t_e increased from 15 to 45 min and 240 to 900 min, respectively, as the bed height increased from 1 to 2 cm (0.308−0.612 g). This can be ascribed to the fact that an increase in bed height increased the surface area of

https://doi.org/10.1021/acsomega.3c05008
ACS Omega 2024, 9, 12564−12574

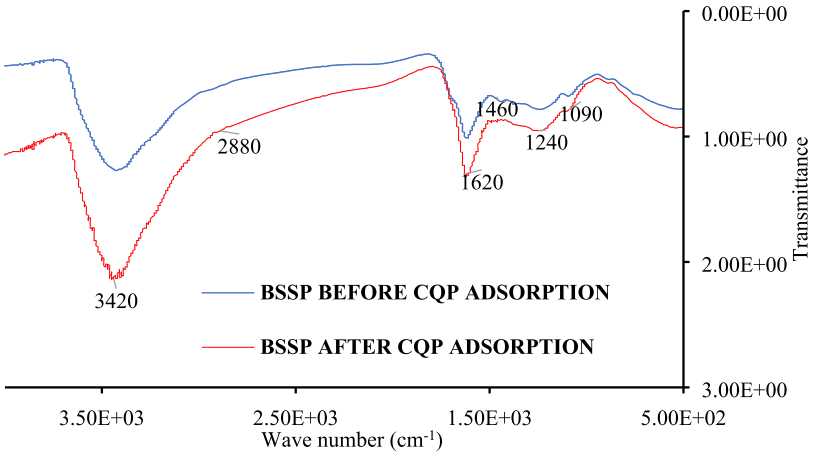

Figure 5. FTIR spectra of BSSPs before and after the uptake of CQP.

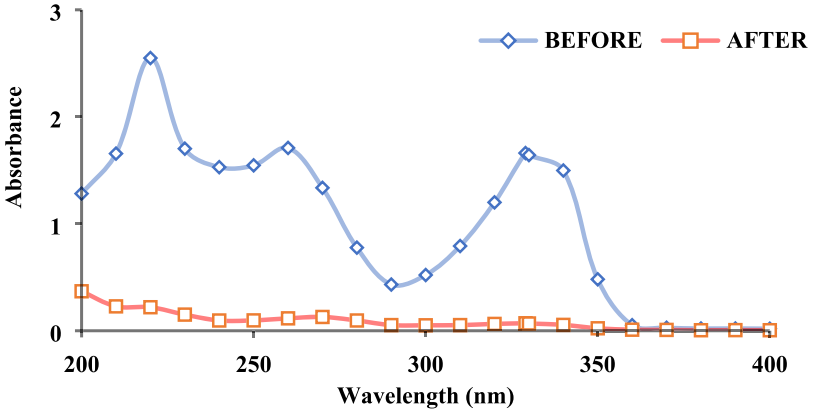

Figure 6. Adsorption of CQP from the simulated multicomponent effluent onto BSSPs (50 mg/L).

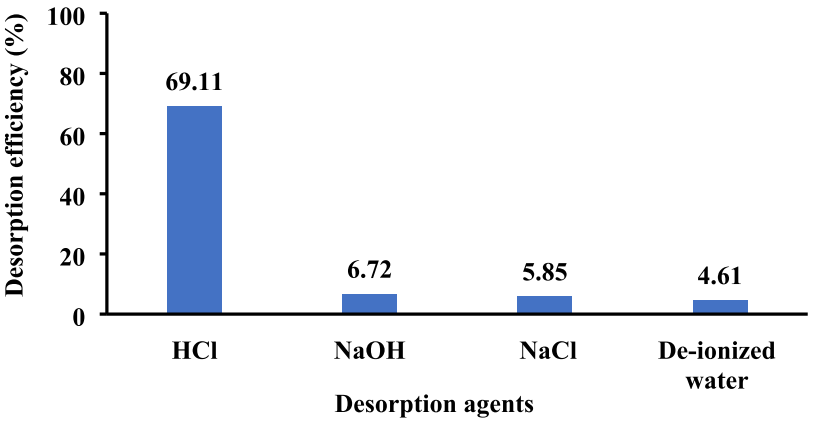

Figure 7. Desorption of CQP from the BSSP surface using different eluents.

BSSPs, which aided the availability of more binding sites for CQP molecules, hence increasing the quantity of CQP adsorbed.[65] The estimated quantity adsorbed for different column operational parameters is presented in Table S2. High removal efficiency has previously been reported on the adsorption of heavy metals using agrowastes.[30]

3.8. Breakthrough Curve Models. *3.8.1. Thomas Model Evaluation for the Uptake of CQP onto BSSPs.* The kinetic coefficients for the Thomas model and the maximum quantity adsorbed (mg/g) in the solid phase were calculated. These parameters were determined by calculating the slope and intercept of the Thomas model plot. The Thomas constant (K_{TH}) decreased as the initial CQP concentration, column bed height, and flow rate increased. This is because the driving force between the CQP molecules and the adsorbent surface has increased.[66] Table S3 lists the evaluated parameters for the Thomas model.

3.8.2. Yoon–Nelson Model Evaluation for the Uptake of CQP onto BSSPs. The estimated parameters for the Yoon–Nelson model for CQP uptake onto BSSPs are presented in Table S4. As observed, as the flow rate increased, the Yoon–Nelson constant, K_{YN}, increased and T decreased. On the other

https://doi.org/10.1021/acsomega.3c05008
ACS Omega 2024, 9, 12564−12574

hand, as the initial concentration increased, the breakthrough time decreased as the column got saturated more rapidly. Also, the values of T_{exp} and T_{cal} were found to be in good agreement with minimal Chi-square (χ^2) error values. Similar trends have been reported.[66,67]

3.9. Treatment of the CQP Simulated Multicomponent Effluent. The simulation of a multicomponent effluent is essential to substantiate the efficiency of BSSPs in the treatment of real industrial effluents. Figure 6 presents the UV−visible spectra of the simulated multicomponent effluent before and after CQP removal onto BSSPs in the company of other contaminants. The percentage removal of the adsorption system was estimated to be 95.78% at the initial CQP concentration of 50 mg/L. The removal efficiencies for other components are presented in Table S5. Similar observations have been reported.[27,28,68] With this estimated performance, BSSPs can serve as an active adsorbent in the treatment of multicomponent pharmaceutical industrial effluents.

3.10. Desorption Studies of the CQP-BSSP Adsorption System. Hydrochloric acid (HCl) had the highest desorption efficiency of 69.11%, while NaOH, NaCl, and deionized water have a desorption efficiency of 6.72, 5.85, and 4.61%, respectively (Figure 7). The BSSP (pH_{pzc} = 3) has the highest adsorption efficiency at pH 8, suggesting that CQP has high activity in slightly basic medium. High desorption efficiency was obtained using a strong acid (HCl) as an eluent via ion exchange. Strong acids and bases have previously been reported to successfully desorb electrostatically attracted adsorbates/molecules.[69] The HCl eluent has a desorption index of 2.95, which is greater than 1. This indicated a high degree of reversibility of the adsorption process.[34] Hence, the feasibility of repeatedly using BSSPs in adsorption processes is a possibility.

4. CONCLUSIONS

Highly porous biochar (BSSPs) was successfully prepared from *B. sapida* wastes. The morphological appearance showed crevices and holes that can trap large molecules, while surface chemistry showed functional groups important in the adsorption process. Thus, BSSPs effectively scavenged CQP in both the batch and fixed-bed adsorption systems for simulated pharmaceutical wastewater. The mechanism of adsorption was found to be dominated by external diffusion. The involvement of the functional groups in the adsorption process was indicated by the variations in the intensity of the FTIR spectra produced before and after the adsorption of CQP. The ANN structure with 11 hidden neurons, Levenberg−Marquardt algorithm, and *Logsig* transfer function was found to be the best parameter combination for predicting the adsorption efficiency. The best operational parameters evaluated from the fixed-bed adsorption studies were 2 cm bed height and 6 mL/min flow rate. The findings of the desorption studies show that BSSPs have a reusability tendency.

ASSOCIATED CONTENT

Supporting Information

The Supporting Information is available free of charge at https://pubs.acs.org/doi/10.1021/acsomega.3c05008.

pH_{pzc} of BSSPs, effect of the initial concentration and contact time on CQP uptake onto BSSPs, breakthrough curves at different flow rates for CQP uptake onto BSSPs, effect of initial CQP concentration on the fixed-bed adsorption onto BSSPs, thermodynamic parameters of CQP uptake onto BSSPs, estimated quantity adsorbed for different column operational parameters, and removal efficiency of pharmaceuticals in the simulated mixture (PDF)

AUTHOR INFORMATION

Corresponding Authors

Adejumoke Abosede Inyinbor − *Department of Physical Sciences, Landmark University, Omu Aran 251101, Nigeria; Clean water and Sanitation Sustainable Development Goal, Landmark University, Omu Aran 251101, Nigeria;* orcid.org/0000-0001-8321-3148; Email: inyinbor.adejumoke@landmarkuniversity.edu.ng

Deborah Temitope Bankole − *Department of Physical Sciences, Landmark University, Omu Aran 251101, Nigeria; Clean water and Sanitation Sustainable Development Goal, Landmark University, Omu Aran 251101, Nigeria;* orcid.org/0000-0003-3281-0502; Email: bankole.deborah@lmu.edu.ng

Author

Abimbola Peter Oluyori − *Department of Physical Sciences, Landmark University, Omu Aran 251101, Nigeria*

Complete contact information is available at: https://pubs.acs.org/10.1021/acsomega.3c05008

Notes

The authors declare no competing financial interest.

ACKNOWLEDGMENTS

The authors are grateful to May and Baker Pharmaceuticals, Lagos, Nigeria, for graciously gifting chloroquine phosphate active and other pharmaceutical actives. The authors also appreciate the proprietor and management of Landmark University for facility provision.

REFERENCES

(1) Haro, N. K.; Dávila, I. V. J.; Nunes, K. G. P.; de Franco, M. A. E.; Marcilio, N. R.; Féris, L. A. Kinetic, Equilibrium and Thermodynamic Studies of the Adsorption of Paracetamol in Activated Carbon in Batch Model and Fixed-Bed Column. *Appl. Water Sci.* **2021**, *11* (2), No. 38.

(2) Inyinbor, A. A.; Bankole, D. T.; Adekola, F. A.; Bello, O. S.; Oreofe, T.; Amone, K.; Lukman, A. F. Chemometrics Validation of Adsorption Process Economy: Case Study of Acetaminophen Removal onto Quail Eggshell Adsorbents. *Sci. Afr.* **2023**, *19*, No. e01471, DOI: 10.1016/j.sciaf.2022.e01471.

(3) De Andrade, J. R.; Oliveira, M. F.; Da Silva, M. G. C.; Vieira, M. G. A. Adsorption of Pharmaceuticals from Water and Wastewater Using Nonconventional Low-Cost Materials: A Review. *Ind. Eng. Chem. Res.* **2018**, *57* (9), 3103−3127.

(4) Ramesh, M.; Anitha, S.; Poopal, R. K.; Shobana, C. Evaluation of Acute and Sublethal Effects of Chloroquine (C18H26CIN3) on Certain Enzymological and Histopathological Biomarker Responses of a Freshwater Fish Cyprinus Carpio. *Toxicol. Rep.* **2018**, *5*, 18−27.

(5) Lin, Y. C.; Lin, J. F.; Wen, S. I.; Yang, S. C.; Tsai, T. F.; Chen, H. E.; Chou, K. Y.; Hwang, T. I. S. Chloroquine and Hydroxychloroquine Inhibit Bladder Cancer Cell Growth by Targeting Basal Autophagy and Enhancing Apoptosis. *Kaohsiung J. Med. Sci.* **2017**, *33* (5), 215−223.

(6) Takano, T.; Katoh, Y.; Doki, T.; Hohdatsu, T. Effect of Chloroquine on Feline Infectious Peritonitis Virus Infection in Vitro and in Vivo. *Antiviral Res.* **2013**, *99* (2), 100−107.

(7) Dada, A. O.; Inyinbor, A. A.; Bello, O. S.; Tokula, B. E. Novel Plantain Peel Activated Carbon−Supported Zinc Oxide Nanocomposites (PPAC-ZnO-NC) for Adsorption of Chloroquine Synthetic Pharmaceutical Used for COVID-19 Treatment. *Biomass Convers. Biorefin.* **2023**, *13*, 9181.
(8) Shen, H.; Wu, N.; Wang, Y.; Zhao, H.; Zhang, L.; Li, T.; Zhao, M. Chloroquine Attenuates Paraquat-Induced Lung Injury in Mice by Altering Inflammation, Oxidative Stress and Fibrosis. *Int. Immunopharmacol.* **2017**, *46*, 16−22.
(9) Wichmann, O.; Eggelte, T. A.; Gellert, S.; Osman, M. E.; Mylius, F.; Ehrhardt, S.; Anemana, S. D.; Bienzle, U.; Mockenhaupt, F. P. High Residual Chloroquine Blood Levels in African Children with Severe Malaria Seeking Healthcare. *Trans. R. Soc. Trop. Med. Hyg.* **2007**, *101* (7), 637−642.
(10) Ramírez-Morales, D.; Masís-Mora, M.; Beita-Sandí, W.; Montiel-Mora, J. R.; Fernández-Fernández, E.; Méndez-Rivera, M.; Arias-Mora, V.; Leiva-Salas, A.; Brenes-Alfaro, L.; Rodríguez-Rodríguez, C. E. Pharmaceuticals in Farms and Surrounding Surface Water Bodies: Hazard and Ecotoxicity in a Swine Production Area in Costa Rica. *Chemosphere* **2021**, *272*, No. 129574.
(11) Khan, H. K.; Rehman, M. Y. A.; Malik, R. N. Fate and Toxicity of Pharmaceuticals in Water Environment: An Insight on Their Occurrence in South Asia. *J. Environ. Manage.* **2020**, *271*, No. 111030.
(12) Bankole, D. T.; Oluyori, A. P.; Inyinbor, A. A. Acid-Activated Hibiscus Sabdariffa Seed Pods Biochar for the Adsorption of Chloroquine Phosphate: Prediction of Adsorption Efficiency via Machine Learning Approach. *S. Afr. J. Chem. Eng.* **2022**, *42*, 162−175.
(13) Inyinbor, A. A.; Bankole, D. T.; Solomon, P. Adsorptive Removal of Acetaminophen onto Acid-Modified Raphia Hookeri Fruit Epicarp. *Biomass Convers. Biorefin.* **2023**, 1−12, DOI: 10.1007/s13399-023-03871-0.
(14) Bello, O. S.; Alao, O. C.; Alagbada, T. C.; Agboola, O. S.; Omotoba, O. T.; Abikoye, O. R. A Renewable, Sustainable and Low-Cost Adsorbent for Ibuprofen Removal. *Water Sci. Technol.* **2021**, *83* (1), 111−122.
(15) Abdullah Sani, N. S.; Ang, W. L.; Mohammad, A. W.; Nouri, A.; Mahmoudi, E. Sustainable Synthesis of Graphene Sand Composite from Waste Cooking Oil for Dye Removal. *Sci. Rep.* **2023**, *13* (1), No. 1931, DOI: 10.1038/s41598-023-27477-8.
(16) Kavitha, B.; Sarala Thambavani, D. Artificial Neural Network Optimization of Adsorption Parameters for Cr(VI), Ni(II) and Cu(II) Ions Removal from Aqueous Solutions by Riverbed Sand. *Iran. J. Chem. Chem. Eng.* **2020**, *39* (5), 203−223.
(17) Afolabi, I. C.; Popoola, S. I.; Bello, O. S. Machine Learning Approach for Prediction of Paracetamol Adsorption Efficiency on Chemically Modified Orange Peel. *Spectrochim. Acta, Part A* **2020**, *243*, No. 118769.
(18) Rasuli, L.; Dehghani, M. H.; Alimohammadi, M.; Yaghmaeian, K.; Rastkari, N.; Salari, M. Mesoporous Metal Organic Frameworks Functionalized with the Amino Acids as Advanced Sorbents for the Removal of Bacterial Endotoxins from Water: Optimization, Regression and Kinetic Models. *J. Mol. Liq.* **2021**, *339*, No. 116801.
(19) Şenol, Z. M. Effective Biosorption of Allura Red Dye from Aqueous Solutions by the Dried-Lichen (Pseudoevernia Furfuracea) Biomass. *Int. J. Environ. Anal. Chem.* **2022**, *102* (16), 4550−4564.
(20) Chen, W. S.; Chen, Y. C.; Lee, C. H. Modified Activated Carbon for Copper Ion Removal from Aqueous Solution. *Processes* **2022**, *10* (1), No. 150.
(21) Ekpete, O. A.; Marcus, A. C.; Osi, V. Preparation and Characterization of Activated Carbon Obtained from Plantain (Musa Paradisiaca) Fruit Stem. *J. Chem.* **2017**, *2017*, No. 8635615.
(22) Temitope Bankole, D.; Peter Oluyori, A.; Abosede Inyinbor, A. Potent Adsorbent Prepared from Bilghia Sapida Waste Material: Surface Chemistry and Morphological Characterization. *Mater. Today Proc.* **2022**, *65* (8), 3665−3670.
(23) Obayomi, K. S.; Lau, S. Y.; Zahir, A.; Meunier, L.; Jianhua, Z.; Dada, A. O.; Rahman, M. M. Removing Methylene Blue from Water: A Study of Sorption Effectiveness onto Nanoparticles-Doped Activated Carbon. *Chemosphere* **2023**, *313*, No. 137533, DOI: 10.1016/j.chemosphere.2022.137533.
(24) Almuntashiri, A.; Hosseinzadeh, A.; Badeti, U.; Shon, H.; Freguia, S.; Dorji, U.; Phuntsho, S. Removal of Pharmaceutical Compounds from Synthetic Hydrolysed Urine Using Granular Activated Carbon: Column Study and Predictive Modelling. *J. Water Process Eng.* **2022**, *45*, No. 102480.
(25) Gharin Nashtifan, S.; Azadmehr, A.; Maghsoudi, A. Comparative and Competitive Adsorptive Removal of Ni2 + and Cu2 + from Aqueous Solution Using Iron Oxide-Vermiculite Composite. *Appl. Clay Sci.* **2017**, *140*, 38−49.
(26) Girish, C. R. Various Isotherm Models for Multicomponent Adsorption: A Review. *Int. J. Civ. Eng. Technol.* **2017**, *8* (10), 80−86.
(27) Saucier, C.; Adebayo, M. A.; Lima, E. C.; Cataluña, R.; Thue, P. S.; Prola, L. D. T.; Puchana-Rosero, M. J.; Machado, F. M.; Pavan, F. A.; Dotto, G. L. Microwave-Assisted Activated Carbon from Cocoa Shell as Adsorbent for Removal of Sodium Diclofenac and Nimesulide from Aqueous Effluents. *J. Hazard. Mater.* **2015**, *289*, 18−27.
(28) Lima, D. R.; Hosseini-Bandegharaei, A.; Thue, P. S.; Lima, E. C.; de Albuquerque, Y. R. T.; dos Reis, G. S.; Umpierres, C. S.; Dias, S. L. P.; Tran, H. N. Efficient Acetaminophen Removal from Water and Hospital Effluents Treatment by Activated Carbons Derived from Brazil Nutshells. *Colloids Surf., A* **2019**, *583*, No. 123966.
(29) Shah, H.; Jain, A.; Laghate, G.; Prabhudesai, D. Pharmaceutical Excipients. *Remington* **2021**, 633−643.
(30) Chowdhury, Z. Z.; Abd Hamid, S. B.; Zain, S. M. Evaluating Design Parameters for Breakthrough Curve Analysis and Kinetics of Fixed Bed Columns for Cu(II) Cations Using Lignocellulosic Wastes. *BioResources* **2015**, *10* (1), 732−749.
(31) Díaz-Blancas, V.; Aguilar-Madera, C. G.; Flores-Cano, J. V.; Leyva-Ramos, R.; Padilla-Ortega, E.; Ocampo-Pérez, R. Evaluation of Mass Transfer Mechanisms Involved during the Adsorption of Metronidazole on Granular Activated Carbon in Fixed Bed Column. *J. Water Process Eng.* **2020**, *36*, No. 101303.
(32) da Costa, T. B.; da Silva, T. L.; Costa, C. S. D.; da Silva, M. G. C.; Vieira, M. G. A. Chromium Adsorption Using Sargassum Filipendula Algae Waste from Alginate Extraction: Batch and Fixed-Bed Column Studies. *Chem. Eng. J. Adv.* **2022**, *11*, No. 100341.
(33) da Silva Alves, D. C.; Healy, B.; Pinto, L. A. d. A.; Cadaval, T. R. S.; Breslin, C. B. Recent Developments in Chitosan-Based Adsorbents for the Removal of Pollutants from Aqueous Environments. *Molecules* **2021**, *26* (3), No. 594.
(34) Dada, A. O.; Adekola, F. A.; Odebunmi, E. O.; Ogunlaja, A. S.; Bello, O. S. Two−Three Parameters Isotherm Modeling, Kinetics with Statistical Validity, Desorption and Thermodynamic Studies of Adsorption of Cu(II) Ions onto Zerovalent Iron Nanoparticles. *Sci. Rep.* **2021**, *11* (1), No. 16454.
(35) Sahin, O. I.; Saygi-Yalcin, B.; Saloglu, D. Adsorption of Ibuprofen from Wastewater Using Activated Carbon and Graphene Oxide Embedded Chitosan−Pva: Equilibrium, Kinetics, and Thermodynamics and Optimization with Central Composite Design. *Desalin. Water Treat.* **2020**, *179*, 396−417.
(36) Bello, O. S.; Adegoke, K. A.; Akinyunni, O. O. Preparation and Characterization of a Novel Adsorbent from Moringa Oleifera Leaf. *Appl. Water Sci.* **2017**, *7* (3), 1295−1305.
(37) Akhtar, J.; Amin, N. A. S.; Shahzad, K. A Review on Removal of Pharmaceuticals from Water by Adsorption. *Desalin. Water Treat.* **2016**, *57* (27), 12842−12860.
(38) Oh, S.; Shin, W. S.; Kim, H. T. Effects of PH, Dissolved Organic Matter, and Salinity on Ibuprofen Sorption on Sediment. *Environ. Sci. Pollut. Res.* **2016**, *23* (22), 22882−22889.
(39) Schrezenmeier, E.; Dörner, T. Mechanisms of Action of Hydroxychloroquine and Chloroquine: Implications for Rheumatology. *Nat. Rev. Rheumatol.* **2020**, *16* (3), 155−166.
(40) Bashir, M.; Mohan, C.; Tyagi, S.; Annachhatre, A. Copper Removal from Aqueous Solution Using Chemical Precipitation and Adsorption by Himalayan Pine Forest Residue as Biochar. *Water Sci. Technol.* **2022**, *86* (3), 530−554.

https://doi.org/10.1021/acsomega.3c05008
ACS Omega 2024, 9, 12564−12574

(41) Njewa, J. B.; Biswick, T. T.; Vunain, E.; Lagat, C. S.; Lugasi, S. O. Synthesis and Characterization of Activated Carbon from Agrowastes for the Removal of Acetic Acid from an Aqueous Solution. *Adsorpt. Sci. Technol.* **2022**, *2022*, 1−13.
(42) Mohamad Zulfika, H. B. Z.; Baini, R.; Ahmad Zauzi, N. S. Effect of PH, Dosage and Concentration on the Adsorption of Congo Red onto Untreated and Treated Aluminium Dross. *IOP Conf. Ser.: Mater. Sci. Eng.* **2017**, *205* (1), No. 012026.
(43) Pauletto, P. S.; Lütke, S. F.; Dotto, G. L.; Salau, N. P. G. Forecasting the Multicomponent Adsorption of Nimesulide and Paracetamol through Artificial Neural Network. *Chem. Eng. J.* **2021**, *412*, No. 127527.
(44) Babalola, B. M.; Babalola, A. O.; Akintayo, C. O.; Lawal, O. S.; Abimbade, S. F.; Oseghe, E. O.; Akinola, L. S.; Ayanda, O. S. Adsorption and Desorption Studies of Delonix Regia Pods and Leaves: Removal and Recovery of Ni(II) and Cu(II) Ions from Aqueous Solution. *Drinking Water Eng. Sci.* **2020**, *13* (1), 15−27.
(45) Eletta, O. A. A.; Mustapha, S. I.; Ajayi, O. A.; Ahmed, A. T. Optimization of Dye Removal from Textile Wastewater Using Activated Carbon from Sawdust. *Nig. J. Technol. Dev.* **2018**, *15* (1), 26.
(46) Khan, T.; Mustafa, M. R. U.; Isa, M. H.; Manan, T. S. B. A.; Ho, Y. C.; Lim, J. W.; Yusof, N. Z. Artificial Neural Network (ANN) for Modelling Adsorption of Lead (Pb (II)) from Aqueous Solution. *Water, Air. Soil Pollut.* **2017**, *228* (11), No. 426, DOI: 10.1007/s11270-017-3613-0.
(47) Silva, M. C.; Spessato, L.; Silva, T. L.; Lopes, G. K. P.; Zanella, H. G.; Yokoyama, J. T. C.; Cazetta, A. L.; Almeida, V. C. H3PO4−Activated Carbon Fibers of High Surface Area from Banana Tree Pseudo-Stem Fibers: Adsorption Studies of Methylene Blue Dye in Batch and Fixed Bed Systems. *J. Mol. Liq.* **2021**, *324*, No. 114771.
(48) Deniz, F.; Kepekci, R. A. Biosorption of Food Green 3 by a Novel Green Generation Composite Biosorbent from Aqueous Environment. *Int. J. Phytorem.* **2017**, *19* (6), 579−586.
(49) Dada, A. O.; Adekola, F. A.; Odebunmi, E. O.; Inyinbor, A. A.; Akinyemi, B. A.; Adesewa, I. D. Kinetics and Thermodynamics of Adsorption of Rhodamine B onto Bentonite Supported Nanoscale Zerovalent Iron Nanocomposite. *J. Phys.: Conf. Ser.* **2019**, *1299* (1), No. 012106.
(50) Chang, J.; Shen, Z.; Hu, X.; Schulman, E.; Cui, C.; Guo, Q.; Tian, H. Adsorption of Tetracycline by Shrimp Shell Waste from Aqueous Solutions: Adsorption Isotherm, Kinetics Modeling, and Mechanism. *ACS Omega* **2020**, *5* (7), 3467−3477.
(51) Kerkhoff, C. M.; da Boit Martinello, K.; Franco, D. S. P.; Netto, M. S.; Georgin, J.; Foletto, E. L.; Piccilli, D. G. A.; Silva, L. F. O.; Dotto, G. L. Adsorption of Ketoprofen and Paracetamol and Treatment of a Synthetic Mixture by Novel Porous Carbon Derived from Butia Capitata Endocarp. *J. Mol. Liq.* **2021**, *339*, No. 117184, DOI: 10.1016/j.molliq.2021.117184.
(52) Tarbuka, P. F.; Gumus, R. H. Methylene Blue and Iron (II) Adsorption onto Raphia Hookeri Seed: A Comparative Equilibrium Isotherm Study. *Int. J. Chem. Process Eng. Res.* **2021**, *8* (1), 11−18.
(53) Ahmed, M.; Mashkoor, F.; Nasar, A. Development, Characterization, and Utilization of Magnetized Orange Peel Waste as a Novel Adsorbent for the Confiscation of Crystal Violet Dye from Aqueous Solution. *Groundwater Sustainable Dev.* **2020**, *10*, No. 100322.
(54) Liu, G.; Dai, Z.; Liu, X.; Dahlgren, R. A.; Xu, J. Modification of Agricultural Wastes to Improve Sorption Capacities for Pollutant Removal from Water − a Review. *Carbon Res.* **2022**, *1*, No. 24.
(55) Ogunmodede, J.; Akanji, S. B.; Bello, O. S. Moringa Oleifera Seed Pod-Based Adsorbent for the Removal of Paracetamol from Aqueous Solution: A Novel Approach toward Diversification. *Environ. Prog. Sustainable Energy* **2021**, *40* (4), 1−11.
(56) Allaoui, M.; Berradi, M.; Taouil, H.; Es-Sahbany, H.; Kadiri, L.; Ouass, A.; Bensalah, J.; Ahmed, S. I. Adsorption of Heavy Metals (Nickel) by the Shell Powder of the Coast of Mehdia-Kenitra (Morocco). *Anal. Bioanal. Electrochem.* **2019**, *11* (11), 1547−1558.
(57) Liu, J.; Cheng, W.; Yang, X.; Bao, Y. Modification of Biochar with Silicon by One-Step Sintering and Understanding of Adsorption Mechanism on Copper Ions. *Sci. Total Environ.* **2020**, *704*, No. 135252.
(58) Mandal, A.; Bar, N.; Das, S. K. Phenol Removal from Wastewater Using Low-Cost Natural Bioadsorbent Neem (Azadirachta Indica) Leaves: Adsorption Study and MLR Modeling. *Sustainable Chem. Pharm.* **2020**, *17*, No. 100308.
(59) Loffredo, E.; Carnimeo, C.; Silletti, R.; Summo, C. Use of the Solid By-Product of Anaerobic Digestion of Biomass to Remove Anthropogenic Organic Pollutants with Endocrine Disruptive Activity. *Processes* **2021**, *9* (11), No. 2018.
(60) Ullah, R.; Iftikhar, F. J.; Ajmal, M.; Shah, A.; Akhter, M. S.; Ullah, H.; Waseem, A. Modified Clays as an Efficient Adsorbent for Brilliant Green, Ethyl Violet and Allura Dyes: Kinetic and Thermodynamic Studies. *Pol. J. Environ. Stud.* **2020**, *29* (5), 3831−3839.
(61) Ojediran, J. O.; Dada, A. O.; Aniyi, S. O.; David, R. O.; Adewumi, A. D. Mechanism and Isotherm Modeling of Effective Adsorption of Malachite Green as Endocrine Disruptive Dye Using Acid Functionalized Maize Cob (AFMC). *Sci. Rep.* **2021**, *11* (1), No. 21498.
(62) Xu, L.; Wang, S.; Zhou, J.; Deng, H.; Frost, R. L. Column Adsorption of 2-Naphthol from Aqueous Solution Using Carbon Nanotube-Based Composite Adsorbent. *Chem. Eng. J.* **2018**, *335*, 450−457.
(63) Yanyan, L.; Kurniawan, T. A.; Zhu, M.; Ouyang, T.; Avtar, R.; Dzarfan Othman, M. H.; Mohammad, B. T.; Albadarin, A. B. Removal of Acetaminophen from Synthetic Wastewater in a Fixed-Bed Column Adsorption Using Low-Cost Coconut Shell Waste Pretreated with NaOH, HNO3, Ozone, and/or Chitosan. *J. Environ. Manage.* **2018**, *226*, 365−376.
(64) Lawal, I. A.; Moodley, B. Fixed-Bed and Batch Adsorption of Pharmaceuticals from Aqueous Solutions on Ionic Liquid-Modified Montmorillonite. *Chem. Eng. Technol.* **2018**, *41* (5), 983−993.
(65) Rafati, L.; Ehrampoush, M. H.; Rafati, A. A.; Mokhtari, M.; Mahvi, A. H. Fixed Bed Adsorption Column Studies and Models for Removal of Ibuprofen from Aqueous Solution by Strong Adsorbent Nano-Clay Composite. *J. Environ. Health Sci. Eng.* **2019**, *17* (2), 753−765.
(66) Nazari, G.; Abolghasemi, H.; Esmaieli, M.; Sadeghi Pouya, E. Aqueous Phase Adsorption of Cephalexin by Walnut Shell-Based Activated Carbon: A Fixed-Bed Column Study. *Appl. Surf. Sci.* **2016**, *375*, 144−153.
(67) Chen, S.; Yue, Q.; Gao, B.; Li, Q.; Xu, X.; Fu, K. Adsorption of Hexavalent Chromium from Aqueous Solution by Modified Corn Stalk: A Fixed-Bed Column Study. *Bioresour. Technol.* **2012**, *113*, 114−120.
(68) Wamba, A. G. N.; Ndi, S. K.; Lima, E. C.; Kayem, J. G.; Thue, P. S.; Costa, T. M. H.; Quevedo, A. B.; Benvenutti, E. V.; Machado, F. M. Preparation, Characterization of Titanate Nanosheet−Pozzolan Nanocomposite and Its Use as an Adsorbent for Removal of Diclofenac from Simulated Hospital Effluents. *J. Taiwan Inst. Chem. Eng.* **2019**, *102*, 321−329.
(69) Sajab, M. S.; Chia, C. H.; Zakaria, S.; Sillanpää, M. Adsorption of Heavy Metal Ions on Surface of Functionalized Oil Palm Empty Fruit Bunch Fibres: Single and Binary Systems. *Sains Malays.* **2017**, *46* (1), 157−165.

https://doi.org/10.1021/acsomega.3c05008
ACS Omega 2024, 9, 12564−12574